A&A 510, A88 (2010)
DOI: 10.1051/0004-6361/200912909

Astronomy & Astrophysics

A cometary origin for CO in the stratosphere of Saturn?

T. Cavalié[1], P. Hartogh[1], F. Billebaud[2,3], M. Dobrijevic[2,3], T. Fouchet[4], E. Lellouch[4], T. Encrenaz[4], J. Brillet[2,3], and G. H. Moriarty-Schieven[5]

[1] Max Planck Institute für Sonnensystemforschung, 37191 Katlenburg-Lindau, Germany
e-mail: cavalie@mps.mpg.de
[2] Université de Bordeaux, Laboratoire d'Astrophysique de Bordeaux (LAB), France
[3] CNRS/INSU, UMR 5804, 33271 Floirac Cedex, France
[4] LESIA, Observatoire de Paris, 92195 Meudon, France
[5] National Research Council, Herzberg Institute of Astrophysics, Victoria, BC V9E 2E7, Canada

Received 17 July 2009 / Accepted 24 November 2009

ABSTRACT

Context. The CO(3–2) line has been observed in the atmosphere of Saturn. The CO(3–2) observation proves that an external source of CO exists in the stratosphere of the planet.
Aims. We attempt to constrain the type and magnitude of the external source of CO in the atmosphere of Saturn, by observing the emission core of the CO(6–5) line.
Methods. We observed the CO(6–5) line at the limbs of Saturn. We analysed the observations by means of a 1-D transport model of the atmosphere of Saturn, coupled with a radiative transfer model.
Results. We obtained a high signal-to-noise ratio spectrum that confirms the existence of an external source of CO in the stratosphere of Saturn. We demonstrated that a cometary origin of CO is the most probable, an impact occurring 220 ± 30 years ago and depositing $(2.1 \pm 0.4) \times 10^{15}$ g of CO above 0.1 mbar. However, we cannot totally reject the possibility of CO originating (at least partially) in a steady source.
Conclusions. Complete photochemical modelling of the oxygen compounds is required to determine realistic error bars of the inferred quantities and to conclude on the origin of CO.

Key words. planets and satellites: individual: Saturn – radio lines: planetary systems

1. Introduction

The detection of H_2O and CO_2 by the Infrared Space Observatory and Spitzer in the stratosphere of the giant planets and Titan (Feuchtgruber et al. 1997; Coustenis et al. 1998; Lellouch et al. 2002; Burgdorf et al. 2006) has proven the existence of an external source of oxygen in the outer Solar System that could be in the form of infalling interplanetary dust particles (IDP), ring and/or satellite particles, or large comets. In contrast, observing CO in the stratosphere of a giant planet does not automatically imply an external origin of this species. There is no condensation sink at the tropopause for CO so that it can be transported to the stratosphere from the deep hot interior of the planet. Therefore, CO can either have an internal origin, an external origin or a combination of both.

A dual origin of CO has already been observed in the atmosphere of Jupiter from infrared spectroscopy (Bézard et al. 2002) and tentatively in the atmosphere of Neptune from (sub)millimetre spectroscopy (Lellouch et al. 2005; Hesman et al. 2007). In both planets, observations and their analysis have led to the conclusion that CO, originating in an external source, was provided to the atmospheres of the planets by large comet impacts, the most recent being the impact of the Shoemaker-Levy 9 (SL9) comet in the atmosphere of Jupiter (Lellouch et al. 1995, 1997; Bézard et al. 2002).

While the situation is still unclear in the atmosphere of Uranus (Encrenaz et al. 2004; Cavalié et al. 2008a), Cavalié et al. (2009) demonstrated using their observations of the CO(3–2) rotational line at 345 GHz that there is an external source of CO in Saturn (not excluding an internal source that is probably weaker than in Jupiter). From their analysis, the authors concluded that this external source possibly had an SL9-like comet impact origin, but they did not reject the possibility of a steady source (interplanetary dust particles or grains from the rings and/or satellites). This first observation of CO in Saturn at submillimetre wavelengths has motivated the observations that we present in this paper. We have targeted the central emission core of a CO line at an even higher frequency (691.473 GHz) to directly probe the stratosphere of Saturn around 1 mbar and thus the external source of CO, while our previous attempt at 345 GHz probed a layer around 10–30 mbar (line in absorption). These observations aim to confirm the presence of an external source of CO and determine the most plausible source: a steady source or a sporadic source.

In this paper, we present the first observations of the CO(6–5) line in Saturn using heterodyne spectroscopy. In Sect. 2, we describe the observations and the data reduction. We then describe our atmospheric and radiative transfer models in Sect. 3 and the results obtained from our modelling in Sect. 4. We discuss them in Sect. 5 and finally present our conclusions in Sect. 6.

2. Observations

2.1. Data acquisition

Observations of Saturn at the frequency of the CO(6–5) line (ν_{6-5} = 691.4730763 GHz) were performed using the *D*-band

Table 1. Summary of Saturn's observations.

Date	τ(183 GHz)	Number of limb scans	% of used scans	Remarks
23 Jan. 2009	0.04–0.05			Observing strategy tests
27 Jan. 2009	0.05–0.06	2	100%	Observing strategy tests and validation
30 Jan. 2009	0.05–0.06	2	50%	50% of the scans lost due to bad pointing
13 Mar. 2009	0.05–0.06	4	50%	50% of the scans lost due to bad pointing
14 Mar. 2009	0.04–0.05	4	75%	25% of the scans lost due to bad pointing

Notes. Indicated: the date of the observations, the zenithal opacity conditions at 183 GHz during the observations, the number of limb scans that have been recorded, the percentage of the scans that have been used in the analysis, and remarks about the performed observations.

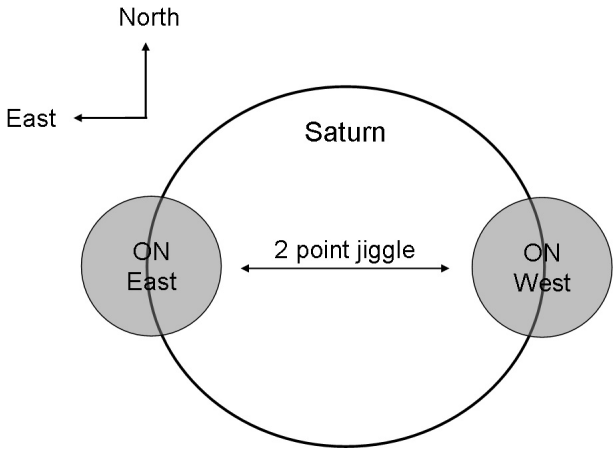

Fig. 1. On-scale scheme representing the 2-point jiggle-map observing mode. The larger disk represents Saturn's disk, while the smaller and filled ones correspond to the antenna beam in each of ON observed positions. The centre of the 7″ beam is alternately centred on the eastern and western limbs and then a common OFF position is observed 60″ away from Saturn's centre in the eastern direction. Eastern and western limb observations were carried out at equatorial latitudes, the sub-earth point latitude being [−3°; −1°] during the observations. *Note:* The rings are not displayed on the figure for simplicity, as they were close to edge-on.

receiver of the James Clerck Maxwell Telescope (JCMT) on 23, 27, and 30 January 2009, and on 13–14 March 2009. The zenithal opacity conditions at 183 GHz (JCMT data) and 225 GHz (Caltech Submillimeter Observatory data) were in the 0.04–0.06 range, i.e., 0.9–1.2 mm of precipitable water vapour, for every single observation, well within the specifications for observations at this frequency (see Table 1).

We carried out the observations with the *D*-band receiver in dual polarization and single-side band mode over a bandwidth of 250 MHz. Our strategy consisted in taking advantage of the relatively small beam (7″) compared to Saturn's size (19.5″×17.5″) and the rapid rotation of the planet, to observe alternately the eastern and western limbs of the planet and then subtract one resulting spectrum from the other. This was performed using a customized 2-point jiggle-map observing mode, in which the eastern and western limbs are observed consecutively as ON positions, both of them sharing a common OFF position observed afterwards (see Fig. 1). Both lines, Doppler-shifted by the rapid rotation of the planet, are thus present in the final spectrum, one with a positive amplitude and the other with a negative amplitude.

The multiple advantages of this "limb-switching" observing technique are the following: i) stronger line contrast; ii) reduction in the amplitude of the baseline ripples; and iii) isolation of the stratospheric line core formed at stratospheric pressure levels around 1 mbar by subtracting the tropospheric wide absorption feature. This technique obviously requires good pointing precision to balance both limb observations efficiently and equilibrate at best the continuum levels. This is why we have not included the spectra for which the difference between the two limbs was too large in our analysis. In the end, 2/3 of the observations were usable (see Table 1).

We also performed short disk-centred observations to measure the continuum level at the frequency of interest. This value is needed to establish a proper flux reference, the continuum level value at the limb being too sensitive to the pointing. Our subsequent analysis was then performed in terms of line-to-continuum ratio.

The *D*-band receiver has two independent channels (A and B). The JCMT staff reported on 27 March 2009 that channel B had a persistent difference in flux with channel A after 20 January 2009, probably caused by the partial vignetting of channel B, that led to a loss of 40% of the flux. From our calibration observations, we established that this difference between the channels has remained constant (within a 5% error bar) over the entire observation period. So, both the disk-centred and the limb observations were affected by the same flux losses in channel B. This is why we chose not to reduce independently the data of the two channels before averaging them, the loss in the disk-centred observations being proportionally the same as the loss in the limb observations.

2.2. Data reduction

The data were processed with the Starlink software of the JCMT. Before combining the different observations, we accounted for the Earth-Saturn relative velocity in the individual spectra (from -20 km s^{-1} in January 2009 to 3 km s^{-1} in March 2009).

After combining the observations, each limb was treated separately before applying the subtraction. The antenna temperature of the continuum at the eastern and western limbs and at the disk-centre are 15.2 K, 11.6 K, and 29.4 K, respectively. The limb values show that there is a small westwards pointing shift, because the difference between them cannot be caused by atmospheric temperature differences at the limbs. By comparing the observed continuum with theoretical computations of the continuum over the planetary disk, we estimate that the average pointing offset on the eastern and western limbs is ∼0.5″. The ratio of the average of the limb values to the disk-centre value is equivalent to the predicted value to within 4%. We rescaled each limb spectrum continuum to the average of the limb continuum values, i.e., 13.4 K, to account for small pointing errors. We then subtracted the western limb spectrum from the eastern limb one and removed a polynomial baseline of third order to obtain the final

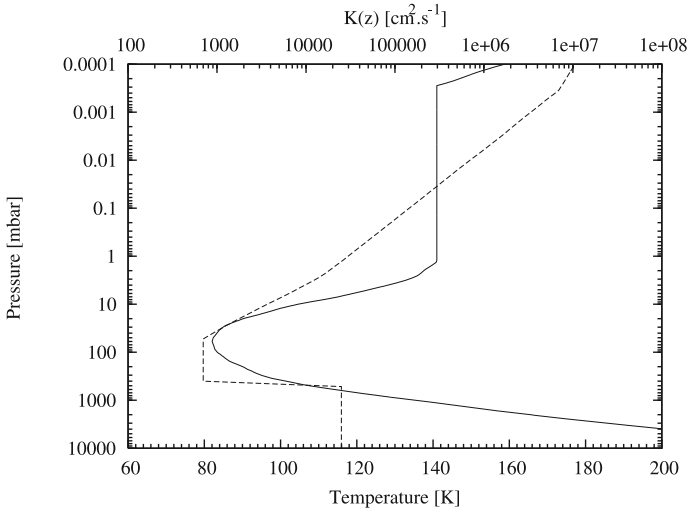

Fig. 2. Temperature (solid line) and eddy diffusion coefficient (dashed line) vertical profiles used in the computations. The $T(z)$ and $K(z)$ profiles come from Ollivier et al. (2000) and Moses et al. (2000a), respectively.

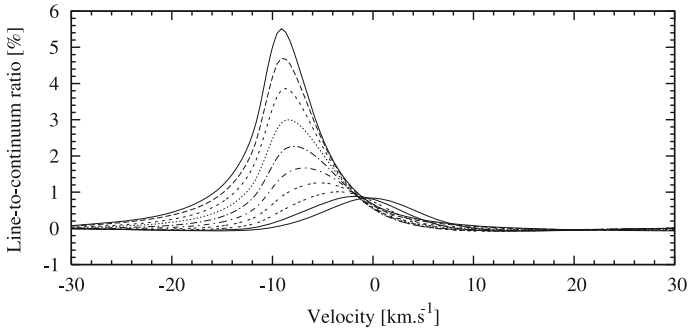

Fig. 3. Beam-integrated spectra, expressed in terms of line-to-continuum ratio, obtained for different lines of sight. The spectrum in solid line with a peak maximum at -9.2 km s^{-1} corresponds to an eastern limb line-of-sight. Other spectra correspond to increasing offsets towards the disk-centre in steps of 1″. The last spectrum (solid line with peak at 0 km s^{-1}) corresponds to a disk-centre line-of-sight. The situation is symmetric on the western side of the disk. This plot shows that the more the beam is pointed towards the disk-centre, the more the line amplitude decreases and the more the line position is shifted towards 0 km s^{-1}. To obtain lines centred around -8.7 km s^{-1} and $+7.7$ km s^{-1}, offsets of 2″ from the eastern limb line-of-sight position and of 5″ from the western limb line-of-sight position, respectively, would be needed.

spectrum. Since the width of the line is ∼17 MHz, we adopted a spectral resolution of 4 MHz to increase the signal-to-noise ratio (*S/N*) without lowering the quality of the lineshape.

We rescaled the continuum of the disk-centred observations to the continuum of our model. So, the final spectrum we present is expressed in terms of the brightness temperature difference between the western and eastern limbs $(\Delta T_b(\nu))_{\rm limbs}$ and

$$(\Delta T_b(\nu))_{\rm limbs} = (\Delta T_a^*(\nu))_{\rm limbs} \times \left(\frac{T_b}{T_a^*}\right)_{\rm disk-centre} \quad (1)$$

where $(\Delta T_a^*(\nu))_{\rm limbs}$ is the difference between the western and eastern limbs on the antenna temperature scale and $(T_b/T_a^*)_{\rm disk-centre}$ is the ratio of the model brightness temperature to the observed antenna temperature in the continuum at the disk-centre.

3. Radiative transfer and atmospheric models

The model we used to perform our radiative transfer analysis was described in Cavalié et al. (2008a) and Cavalié et al. (2009). It is a 1D line-by-line model that accounts for the ellipticity of the planet. The limb emission is taken into account. Here, we chose, for simplicity, not to account for the absorption and emission of the rings, because the ring inclination was always lower than 3°.

We compared the synthetic spectra computed from our radiative transfer model with our observations. The shape of the synthetic spectra depends on the vertical profile of CO. The vertical profile that enabled us to retrieve the CO abundance at the levels that we probed were generated by the 1D time-dependent transport model of the atmosphere of Saturn of Cavalié et al. (2009). The parameters that we fixed prior to our analysis were the CO mixing ratio at the lower boundary $q_{\rm co}$, the atmospheric thermal profile $T(z)$, and the eddy diffusion coefficient vertical profile $K(z)$. The value of $q_{\rm co}$ was set to be zero in every case, except in the internal-source-only model (see Sect. 4). The $T(z)$ profile was taken from Ollivier et al. (2000) and the $K(z)$ profile from Moses et al. (2000a). Both profiles are displayed in Fig. 2. The effect of the uncertainties on $T(z)$ and $K(z)$ will be discussed in Sects. 4 and 5.

We considered two types of external source models: a steady source model and a sporadic source model. We used the same formalism as Cavalié et al. (2009). In the case of the steady source model, we attempted to derive the disk-averaged CO external flux from the observations, while we tried to derive the impact time t_0 and the CO mixing ratio q_0 that would be deposited above 0.1 mbar by an SL9-like comet. The value of q_0 is also disk-averaged (see Cavalié et al. 2008b; and Cavalié et al. 2009, for further details of the modelling).

4. Results

The line was unambiguously detected independently on both limbs ($S/N > 5$ for each observing date). In the final spectrum, we obtain a peak-to-peak *S/N* of 25 at 4 MHz resolution. The eastern limb peak occurs at -8.7 km s^{-1} (close to the predicted velocity of -9.2 km s^{-1}), while the western limb peak is centred on $+7.7$ km s^{-1}. This result is not caused by the averaged pointing offset of ∼0.5″. To obtain this velocity shift, the beam centre of the eastern observation would have to be shifted by 5″ towards the centre of the disk (see Fig. 3). This seems inconsistent because continuum values show that the pointing error is lower than 1″ on both limb observations. This shift could be caused by strong stratospheric winds. However, the prograde stratospheric thermal winds measured by Cassini/CIRS (Liming et al. 2008) are inconsistent with those inferred from our observations, possibly indicating that the forcing of the circulation in Saturn's atmosphere is not purely thermal. We need to include retrograde winds of ∼450 m s^{-1} at the eastern limb and ∼850 m s^{-1} at the western limb to reproduce the lines. Finally, the shift could also be partly caused by the subtraction process and the limitation in the *S/N* of the observations. We are presently unable to say unambiguously why this shift is observed. So, in our analysis, we fitted both limbs as if they were located at their predicted velocity.

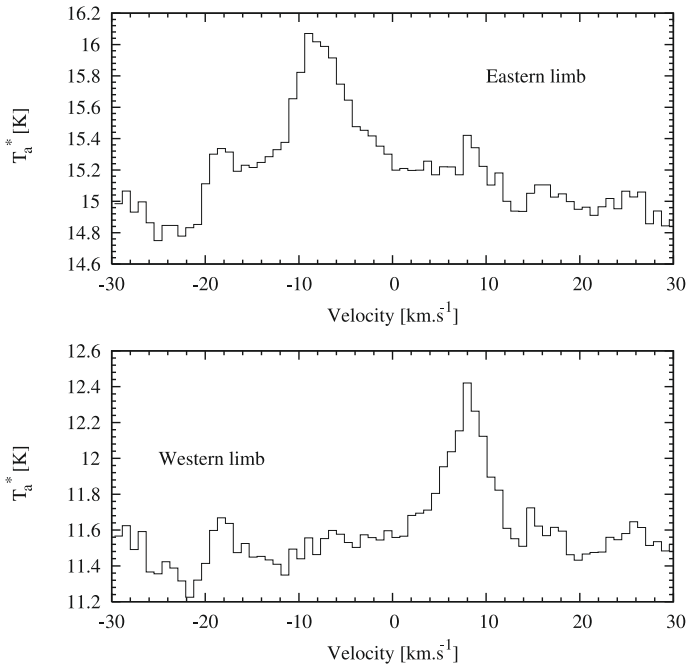

Fig. 4. Raw spectra at the eastern (*top*) and western (*bottom*) limbs of Saturn at the CO(6–5) frequency in terms of antenna temperature as a function of velocity.

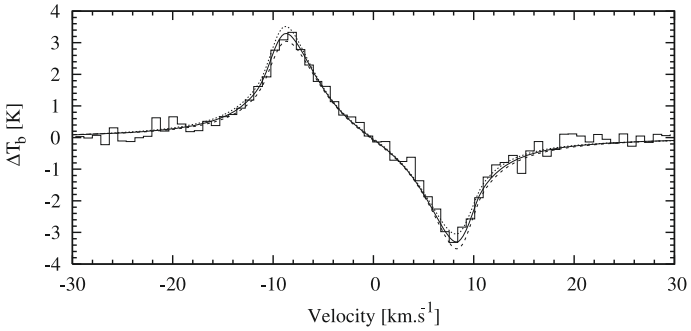

Fig. 5. Effects of a pointing error of −0.5″ (dashed line) and +0.5″ (dotted line) on the modelled spectrum. The solid line represents a comet-impact model with $(q_0, t_0) = (3.5 \times 10^{-6}, 220$ years). We note that the centre of the peaks is shifted only by ∼±0.1 km s^{-1} with these pointing shifts.

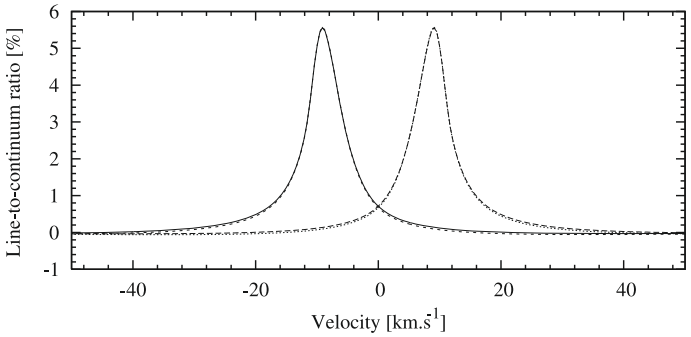

Fig. 6. Spectra of the CO(6–5) line for at the eastern and western limbs for two models, expressed in terms of line-to-continumm ratio. The spectra have been computed for a comet impact model (eastern limb in solid line and western limb in long-dashed line) and for the same comet impact model in which an internal source of CO with a deep mixing ratio of 10^{-9} has been added (eastern limb in short-dashed line and western limb in dotted line). These plots show that an internal source only changes the line-to-continuum ratio in a negligible way since the results for the different models are hardly distinguishable.

4.1. Uncertainty analysis

The main source of uncertainty in the CO abundance measurement comes from the pointing uncertainty of ∼0.5″. Depending on the pointing accuracy, the antenna temperature continuum level at the disk-centre varies slightly. The relative uncertainty in the observed brightness temperature contrast of the line $(\Delta T_b)_{\rm limbs}$ depends linearly on the relative uncertainty in the antenna temperature at the disk-centre $(T_a^*)_{\rm disk-centre}$ and on the uncertainty in the peak-to-peak line contrast $(\Delta T_a^*)_{\rm limbs}$. From Eq. (1), we derive

$$\frac{\sigma\left[(\Delta T_b)_{\rm limbs}\right]}{(\Delta T_b)_{\rm limbs}} = \frac{\sigma\left[(\Delta T_a^*)_{\rm limbs}\right]}{(\Delta T_a^*)_{\rm limbs}} + \frac{\sigma\left[(T_a^*)_{\rm disk-centre}\right]}{(T_a^*)_{\rm disk-centre}}. \quad (2)$$

The peak-to-peak *S/N* being 25, the value of the first term in the equation is 4%. From our repeated measurements, we find a relative uncertainty of 10.5% in the value of $(T_a^*)_{\rm disk-centre}$, leading to a total relative uncertainty in the brightness temperature line contrast of 15%.

This pointing uncertainty also causes some uncertainty in the modelling of the line. So, we checked how the modelled line strength is influenced by pointing errors of ±0.5″. We modelled the limb emission on both limbs with pointing shifts of ±0.5″ and applied the same subtraction procedure as applied to the data to obtain values that could be compared. In the end, a pointing error of 0.5″ in the modelling produces an uncertainty corresponding to 5% of the line contrast (see Fig. 5).

The subtraction process removes information contained in the far wings of the line and thus about the abundance of CO and/or the temperature at altitude levels lower than those probed by the emission core. However, we note that the first observations were performed for a 1 GHz band and that no wide feature could be observed from the individual limb observations.

We also checked whether neglecting the CO produced by a potential internal source (by modelling the CO distribution due to the external source only) would generate an error in the line-to-continuum ratio or not. We therefore computed the line for two kinds of models, the first being the comet impact model with no internal source, and the second the comet impact model with an internal source characterized by a mixing ratio of 10^{-9}, which corresponded to the upper limit derived by Cavalié et al. (2009) and the mixing ratio necessary to account for the 5 μm observations in the case of the internal origin model for CO of Noll & Larson (1991), to check whether the line-to-continuum ratio was changed. Figure 6 shows that the line-to-continuum ratio of each limb changes only negligibly.

The thermal profile of Saturn shows more variations as a function of latitude at low pressures than at higher pressures (Fletcher et al. 2007). Given the size of the antenna beam (7″), that we target the eastern and western limbs, and that the sub-Earth point latitude was always between −1° and −3°, we considered the variations in temperature between −30° and 30°: $\Delta T \sim 2$–3 K if $p > 35$ mbar, and $\Delta T \sim 5$ K if $p < 6$ mbar (Fletcher et al. 2007). An uncertainty of 5 K in the thermal profile seems therefore to be reasonable. By shifting the entire thermal profile by ±5 K, the relative uncertainty in the modelled line contrast is about 4%. If we shift only the upper part ($p < 1$ mbar) of the thermal profile by ±5 K, then the uncertainty in the modelled line contrast reaches 11%. This is still lower than the error bars related to our observing technique.

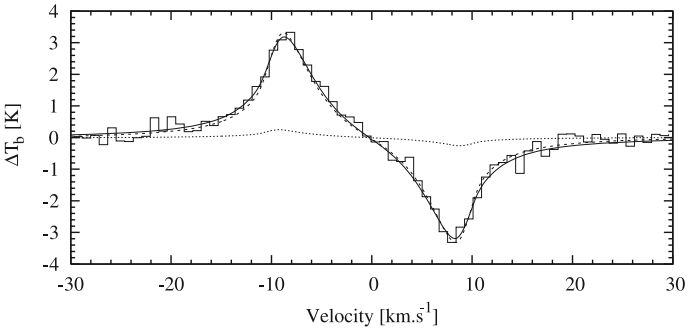

Fig. 7. Limb-switched spectrum of Saturn centred around Saturn's velocity compared to various models. From the observations, an external source is evident since an internal source of CO ($q_{co} = 10^{-9}$, uniform with altitude) results in the dotted line synthetic spectrum. A steady flux of CO of $\phi_{co} = 4.1 \times 10^6$ cm^{-2} s^{-1} results in the dashed line. An SL9-like comet impact model with the parameters (q_0, t_0) = (3×10^{-6}, 200 years) is shown in solid line.

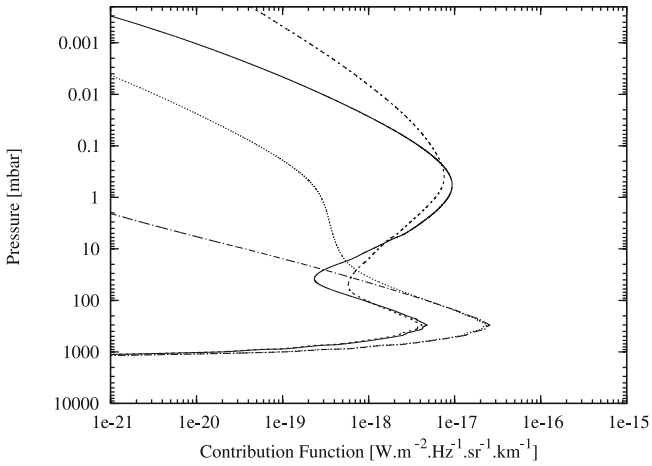

Fig. 8. Contribution functions (not integrated over the beam) of the central emission core of the CO(6–5) line as a function of pressure, computed for a limb line-of-sight (at the centre of the beam) and smoothed to a resolution of 4 MHz. The solid line corresponds to the SL9-like comet impact model ($q_0 = 3 \times 10^{-6}$, $t_0 = 200$ years), which reproduces the CO(6–5) observation. The dashed line correponds to the best-fit steady source model for the CO(6–5) observation (flux of 4.1×10^6 cm^{-2} s^{-1} CO molecules). For comparison, the contribution function for the internal source model ($q_{co} = 10^{-9}$) and a model without any CO are represented by the dotted and dashed-dotted lines, respectively.

Another source of uncertainty in the derivation of model parameters is the $K(z)$ profile in the stratosphere. The $K(z)$ profile was set so as to produce abundance vertical profiles that result in the closest possible match with the observations of hydrocarbons (Moses et al. 2000a). However, the constraints placed on $K(z)$ by hydrocarbons strongly depend on the set of chemical constants that are used in the chemical scheme of the photochemical model. The retrieved $K(z)$ depends on the uncertainties in the chemical constants of the photochemical model as shown by Dobrijevic et al. (2003). The uncertainty in the $K(z)$ profile can reach an order of magnitude. In this work, we did not investigate the effect of this uncertainty. We will investigate the uncertainty in the $K(z)$ profile in a future paper, where we will also take all the photochemical processes into account.

4.2. Determination of external source parameters

First, we underline that the CO line is unambiguously produced by an external source of CO. Figure 7 compares the data with the synthetic line data computed from an internal source model in which the CO mixing ratio is 10^{-9} and uniform with altitude (upper limit derived by Cavalié et al. 2009; as well as mixing ratio necessary to account for the 5 μm observations in the case of the internal origin model for CO of Noll & Larson 1991). This model produces a line that is ~20 times fainter than that inferred from the observed line contrast. So, the contribution of an internal source is negligible in the spectrum. Hereafter, we will focus on models with an external source only and derive the parameters of these models (i.e., flux or comet mass and impact time).

For a steady flux of CO generated by either interplanetary dust particles or a local source, we derive a ϕ_{co} value of $(4.1 \pm 0.6) \times 10^6$ cm^{-2} s^{-1} (see spectrum in Fig. 7). When the CO originates from an SL9-like event, the CO line is mainly sensitive to two parameters, the volume mixing ratio q_0 deposited above the 0.1 mbar level and the time elapsed since the impact t_0. The values that provide the best fit to the CO(6–5) spectrum are (q_0, t_0) = ($[3.0 \pm 0.6] \times 10^{-6}$, 200^{+50}_{-40} years).

5. Discussion

The central emission core of the CO(6–5) rotational line that we have observed is sensitive only to the stratospheric CO distribution (see Fig. 8). We have shown that an internal source only of CO ($q_{co} = 10^{-9}$) cannot account for the line contrast that we have observed. Therefore, we cannot place any additional constraint on the strength of the internal source of CO in the atmosphere of Saturn.

Prior to a discussion about the external source of CO in Saturn, we need to understand what the contribution functions tell us for the CO(6–5) line. Because we also used the results presented in Cavalié et al. (2009), we analysed the contribution functions of the CO(3–2) lines. The contribution functions corresponding to the central frequency of the CO(6–5) line at the planetary limb (beam central line-of-sight) are shown in Fig. 8. They show where the observed emission core is formed. We computed the contribution functions both for the internal and external source models and for a CO free atmosphere model (for comparison). The contribution functions of the CO(6–5) line clearly show that the emission line is formed at pressures of ~1 mbar. The second peak of these functions, which is centred between 100 and 1000 mbar, causes the continuum emission. Theoretically, the CO(3–2) line centre probes also up to the same region. The central emission seen in the external models of the line in Cavalié et al. (2009, see their Figs. 9 and 11) is formed in this region. However, because the *S/N* is low, it is not possible to constrain the CO abundance in this region as precisely as with the CO(6–5) line presented in this paper, whose *S/N* is much higher. Most of the central emission peak contrasts modelled for the CO(3–2) are smaller than the noise level. On the other hand, the CO(3–2) line shows a distinctive absorption feature in disk-centre geometry[1]. To show where the CO(3–2) absorption is formed, we have computed the contribution functions at 20 MHz from the line centre on a disk-centred line-of-sight for several models presented in Cavalié et al. (2009), from which we have subtracted the contribution function obtained from a CO free atmosphere model (see Fig. 9). This has enabled us to remove the

[1] The line forms in a region where the temperature is lower than the continuum temperature, leading to an absorption feature.

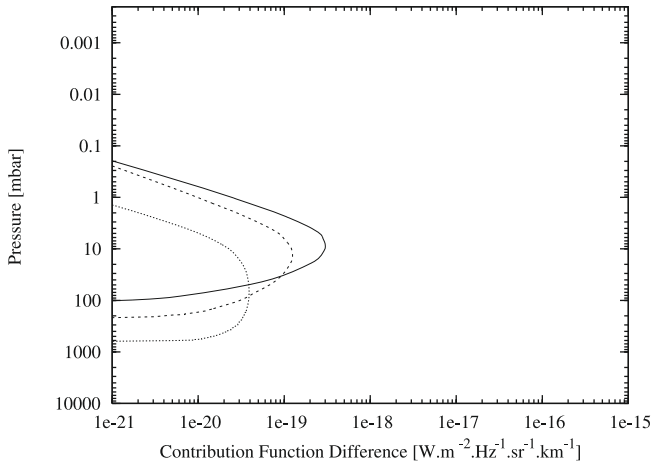

Fig. 9. The different lines plotted result from the subtraction of the contribution function obtained for a CO free atmosphere in the contribution functions obtained from several models for a disk-centred line-of-sight. We have plotted these functions at 20 MHz from the central frequency to focus on the observed absorption feature. Here, the curves corresponding to a comet impact ($q_0 = 3\times10^{-6}$, $t_0 = 250$ years) and to an external steady source of CO ($\phi_{co} = 1.5\times10^6$ cm^{-2} s^{-1}) are the solid and the dashed lines, respectively. The dotted curve refers to an internal source model ($q_{co} = 10^{-9}$). *Note:* The contribution functions used here have not been integrated over the beam but have been smoothed to the spectral resolution of the observation (16 MHz).

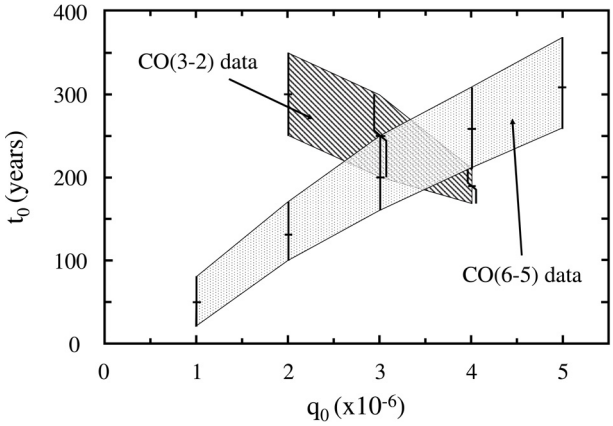

Fig. 10. Parameters q_0 and t_0 in the case of an SL9-like comet impact derived from the CO(6–5) observations (red dotted area, this work). The parameters retrieved by Cavalié et al. (2009) from CO(3–2) observations using the same modelling are also shown for cross-comparison (blue dashed area).

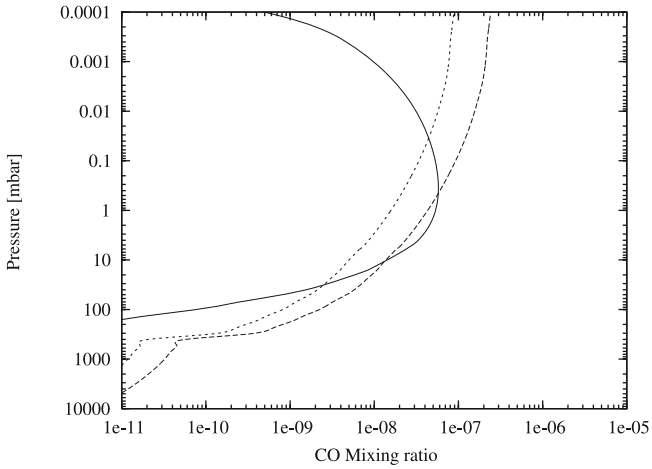

Fig. 11. CO mixing ratio vertical profiles of several external source models. The solid line corresponds to the profile obtained for a comet impact 220 years ago, with $q_0 = 3.5\times10^{-6}$. This model reproduces the CO(3–2) observations and the CO(6–5) observation as well. The long-dashed and short-dashed lines correspond to steady source models with $\phi_{co} = 4.1\times10^6$ cm^{-2} s^{-1} (CO(6–5) line best match) and $\phi_{co} = 1.5\times10^6$ cm^{-2} s^{-1} (CO(3–2) line closest match), respectively.

continuum contribution and thus focus on the CO contribution. We have chosen to plot the contribution functions at 20 MHz from the central frequency to avoid the central emission core. In Cavalié et al. (2009), the models that most successfully reproduce the line are a cometary model for which $q_0 = 3\times10^{-6}$ and $t_0 = 250$ years (solid line in Fig. 9) and a steady source model for which $\phi_{co} = 1.5\times10^6$ cm^{-2} s^{-1} (dashed line in Fig. 9). Finally, these contribution functions indicate where the observed absorption line originates: it is formed around 10 mbar. In the end, the CO(6–5) observation probes pressures centred around 1 mbar on the limb, while the 20 MHz wings of the CO(3–2) line at the disk-centre probe a layer centred around 10 mbar. So, using both observations enables us to retrieve vertical information about the CO distribution at two different pressure levels.

From the SL9-like comet impact model, an entire set of (q_0, t_0) couples, shown in Fig. 10, produces models that match the line. At the frequency of the CO(6–5) line, the higher q_0, the longer t_0 must be to provide a satisfactory fit to the data. In contrast, the lower q_0, the longer t_0 must be to match the CO(3–2) spectrum obtained by Cavalié et al. (2009). So, the possible values of t_0 as a function of q_0 exhibit different behaviour depending on the observed line (see Fig. 10). This result comes from the pressure levels that are probed by these lines being different, as mentioned previously. The abundance of CO decreases with time at the pressure levels probed by the CO(6–5) emission line, whereas it increases with time at the pressure levels probed by the CO(3–2) absorption line.

Figure 10 shows that the set of values for (q_0, t_0) that we derive for the CO(6–5) line overlaps with the set of values derived from the observations of the CO(3–2) line by Cavalié et al. (2009). This overlap is close to the location of our preferred values for (q_0, t_0), i.e., ($[3.5\pm0.5]\times10^{-6}$, 220 ± 30 years). The corresponding CO mixing ratio vertical profile is shown in Fig. 11, and the resulting spectra at the CO(3–2) and CO(6–5) frequencies are shown in Fig. 12. This result confirms that a cometary origin for the CO present in the stratosphere of Saturn is possible. The mass of CO deposited by the comet would be $(2.1\pm0.4)\times10^{15}$ g, corresponding to approximately 3 times the mass of SL9 (Moreno et al. 2003). Collisions of such comets with Saturn occur once every ~750 years, according to Zahnle et al. (2003).

For a steady source of CO, a flux of $\phi_{co} = (4.1\pm0.6)\times10^6$ cm^{-2} s^{-1} is required to fit the CO(6–5) line observations (vertical profile shown in Fig. 11). This value is inconsistent with the flux retrieved with the same model from the CO(3–2) observations, i.e., $\phi_{co} = (1.5\pm0.4)\times10^6$ cm^{-2} s^{-1} (Cavalié et al. 2009). Figure 12 clearly shows that a flux of 4.1×10^6 cm^{-2} s^{-1} results in far too deep absorption at the CO(3–2) frequency and that a flux of 1.5×10^6 cm^{-2} s^{-1} underestimates the CO(6–5) emission. This inconsistency is caused by different layers being probed by the two observed lines, so that the fluxes needed to account for the observed CO at each layer are also different. So, using the assumed $K(z)$ eddy-diffusion coefficient vertical-profile ensures that a steady source seem less likely, compared to the comet impact model results.

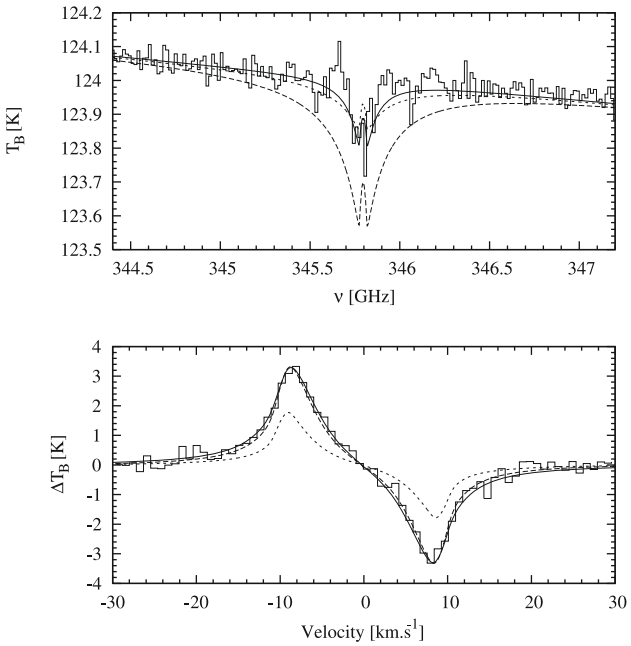

Fig. 12. Spectra of the CO(3–2) line (*top*) and the CO(6–5) line (*bottom*). The only model that fits both lines is the comet impact model in which (q_0, t_0) = (3.5×10^{-6}, 220 years). It is plotted as a solid line. The external steady source model fails to reproduce both lines with the same flux. A flux of 1.5×10^{6} cm^{-2} s^{-1} CO molecules would be needed at the CO(3–2) frequency (short-dashed line), whereas a flux of 4.1×10^{6} cm^{-2} s^{-1} CO molecules would be needed at the CO(6–5) frequency (long-dashed line). *Note*: The layout for each model corresponds to that of Fig. 11, where the corresponding vertical profiles are shown.

6. Conclusion

We have obtained the first observation of the CO(6–5) line in the atmosphere of Saturn from "limb-switching" observations with the JCMT. We have analysed our data by applying a 1-D transport model coupled with a radiative transfer model and tested several hypothese for the possible origin of CO in the atmosphere of the planet.

The first outcome of this work is that an internal source of CO with $q_{co} = 10^{-9}$, corresponding to the upper limit determined by Cavalié et al. (2009), cannot explain the observed emission features, thus confirming that there is an external source of CO in the stratosphere of Saturn. A steady flux of CO of $(4.1 \pm 0.6)\times10^{6}$ cm^{-2} s^{-1} produces a synthetic line that matches the observations as well as a sporadic input of CO that would have been caused by the collision of a SL9-like comet ~200 years ago.

We have then compared our results with the results obtained by observing the CO(3–2) absorption line by Cavalié et al. (2009). Because these lines probe different pressure levels, we have been able to constrain the CO vertical profile more precisely than possible before. Our analysis now clearly favours a cometary origin for CO in the stratosphere of Saturn with model parameters $q_0 = (3.5\pm0.5)\times10^{-6}$ and $t_0 = 220\pm30$ years, resulting in a deposition of $(2.1 \pm 0.4)\times10^{15}$ g of CO. In contrast, the steady source model infers inconsistent values for the CO flux for the CO(3–2) and CO(6–5) observations.

However, we cannot firmly reject the possibility that CO originates (at least partially) in a steady source, because accounting for the photochemistry of H_2O would result in the production of CO (Moses et al. 2000b) and would thus modify the CO vertical profile and affect the flux values. It is unclear at which levels the CO is produced from H_2O, but the effects of CO production from H_2O photochemistry on the spectrum of Saturn at 345 GHz and 691 GHz should depend on the CO production rate vertical profile and on the $K(z)$ profile. Confirmation of this is beyond the scope of this present paper and is left to future analysis.

At the frequencies of H_2O and CO, observations of Saturn will be conducted by the HIFI instrument of the Herschel Space Observatory (Hartogh et al. 2009). These observations should produce very high *S/N* observations of H_2O and CO that will enable us to obtain their vertical profiles with unprecedented accuracy. Photochemical modelling of the oxygen compounds in the atmosphere of Saturn will thus gain precision and enable us to test the validity of the models presented in this paper.

Acknowledgements. T. Cavalié would like to thank the people at JCMT who helped in achieving this project: B. Warrington and J. Hoge for successfully operating the observations, T. Jenness and S. Hart for creating the customized 2-point jiggle mapping observation procedure, J. Dempsey, P. Friberg and K. Brown for re-commissioning the *D*-band receiver in the months prior to our run, and finally I. Coulson for supporting the project from the scheduling phase until the data reduction phase. We also thank the anonymous reviewer for constructive comments on the manuscript.

References

Bézard, B., Lellouch, E., Strobel, D., Maillard, J.-P., & Drossart, P. 2002, Icarus, 159, 95
Burgdorf, M., Orton, G., van Cleve, J., Meadows, V., & Houck, J. 2006, Icarus, 184, 634
Cavalié, T., Billebaud, F., Fouchet, T., et al. 2008a, A&A, 484, 555
Cavalié, T., Billebaud, F., Biver, N., et al. 2008b, Planet. Space Sci., 56, 1573
Cavalié, T., Billebaud, F., Dobrijevic, M., et al. 2009, Icarus, 203, 531
Coustenis, A., Salama, A., Lellouch, E., et al. 1998, A&A, 336, L85
Dobrijevic, M., Ollivier, J. L., Billebaud, F., Brillet, J., & Parisot, J. P. 2003, A&A, 398, 335
Encrenaz, T., Lellouch, E., Drossart, P., et al. 2004, A&A, 413, L5
Feuchtgruber, H., Lellouch, E., de Graauw, T., et al. 1997, Nature, 389, 159
Fletcher, L. N., Irwin, P. G. J., Teanby, N. A., et al. 2007, Icarus, 189, 457
Hartogh, P., Lellouch, E., Crovisier, J., et al. 2009, Planet. Space Sci., 57, 1596
Hesman, B. E., Davis, G. R., Matthews, H. E., & Orton, G. S. 2007, Icarus, 186, 342
Lellouch, E., Paubert, G., Moreno, R., et al. 1995, Nature, 373, 592
Lellouch, E., Bézard, B., Moreno, R., et al. 1997, Planet. Space Sci., 45, 1203
Lellouch, E., Bézard, B., Moses, J. I., et al. 2002, Icarus, 159, 112
Lellouch, E., Moreno, R., & Paubert, G. 2005, A&A, 430, L37
Liming, L., Gierasch, P. J., Achterberg, R. K., et al. 2008, Geophys. Res. Lett., 35, 23208
Moreno, R., Marten, A., Matthews, H. E., & Biraud, Y. 2003, Planet. Space Sci., 51, 591
Moses, J. I., Bézard, B., Lellouch, E., et al. 2000a, Icarus, 143, 244
Moses, J. I., Lellouch, E., Bézard, B., et al. 2000b, Icarus, 145, 166
Noll, K. S., & Larson, H. P. 1991, Icarus, 89, 168
Ollivier, J. L., Dobrijevic, M., & Parisot, J. P. 2000, Planet. Space Sci., 48, 699
Zahnle, K., Schenk, P., Levison, H., et al. 2003, Icarus, 163, 263